Large-grain, oriented, and thin zeolite MFI films

from directly-synthesized nanosheet coatings

Donghun Kim, Meera Shete, Michael Tsapatsis*

Department of Chemical Engineering and Materials Science, University of Minnesota,

Minneapolis, Minnesota 55455 United States

Zeolite MFI film, epitaxial growth, microstructure, crystal growth, nanosheet

Abstract Directly-synthesized zeolite MFI nanosheets are promising building blocks for MFI thin films with large and oriented grains. The secondary growth of MFI nanosheets on Si wafers in tetraethylammonium hydroxide (TEAOH) silica sols was investigated, and conditions that result in well-oriented and intergrown film microstructure were established. This has enabled the fabrication of thin (\sim 300 nm) *b*-oriented MFI films with large grain-size (>2 μ m) from seed-removed nanosheet monolayer coatings. Moreover, the faceted and anisotropic shape of MFI nanosheets allowed the measurement of MFI growth in different crystallographic directions and confirmed the twinning-free preferential growth along the *c*-axis (a lateral direction of the nanosheet), compared to the *b*-axis (the direction normal to the nanosheet basal plane), with ratios in a range between 4–11.

Introduction

In addition to numerous existing applications based on the powder form of zeolites, 1,2 new applications, 3-5 such as membrane separations, 6,7 low-k materials, 8,9 protective coatings (anticorrosion^{10–12} or anti-bacterial¹³), and sensing^{14,15} have been explored using zeolite films. Zeolite films are also desirable for advanced characterization of zeolite catalytic and transport properties. 16,17 Among various zeolites, MFI has been extensively studied to be fabricated as oriented thin films. These efforts include control of film thickness, 18 crystal orientation, 19 grain size, 20 and chemical composition. 21 Secondary growth of seed crystals deposited on the substrate is an effective method to achieve the desired microstructures. 22-25 It was used to fabricate oriented MFI thin films with aligned straight channels perpendicular to the substrate, based on synthesis of shaped seed crystals, ²⁶ fabrication of uniform and dense seed crystal coatings, ^{27,28} and epitaxial secondary growth. 29-32 In particular, MFI nanosheets prepared from the exfoliation³³ of multi-lamellar MFI material³⁴ enabled the fabrication of ultra-thin oriented MFI films (~12 nm).³⁵ However, the grain sizes were limited to below a few hundred nanometers. Large lateral size of the grain is desirable for MFI thin films, as it reduces the density of grain boundaries and is expected to yield single-crystal-like properties (e.g., dielectric constant and elastic modulus³⁶).

Recently-reported directly-synthesized MFI nanosheets, ²⁰ in comparison to exfoliated nanosheets, have large lateral dimensions (>2 μm) and were used to fabricate high-performance MFI separation membranes with large grain sizes. However, these MFI membranes were prepared from multi-layer nanosheet coatings. ^{20,28} A film or membrane made from a monolayer of MFI nanosheets is desirable because it will provide continuous (uninterrupted) straight channels along its thin dimension. Here, we report progress in this direction based on the

anisotropic epitaxial growth of directly-synthesized MFI nanosheets in a tetraethylammonium hydroxide (TEAOH) silica sol. Growth in different crystallographic directions is quantitated, and oriented MFI films with in-plane grain sizes larger than 2 μ m and thickness of ~300 nm is reported for the first time.

Experimental Section

Synthesis of MFI nanosheets MFI nanosheets were synthesized by seeded growth with bis-1,5(tripropyl ammonium) pentamethylene diiodide (dC5), as reported previously.²⁰ In brief, a precursor sol with a composition of 80TEOS: 3.75dC5: 20KOH: 9500H₂O was hydrolyzed for 16 h under ambient conditions. After filtered with a 0.45-μm GHP (polypropylene) syringe filter, the precursor sol was mixed with a suspension of MFI nanocrystals at 1000:1 silica ratio of precursor sol to nanocrystal suspension. The mixture was then placed in a TeflonTM-lined stainless steel autoclave and hydrothermally treated at 140 °C for 4 days. As-synthesized MFI nanosheets were purified with centrifugation to remove aggregates and re-dispersed in DI water containing 5–10 vol% ethanol.²⁸

Coating of MFI nanosheets on Si substrates MFI nanosheets were first deposited at the airwater interface and then transferred on Si substrates. The amount of MFI nanosheet dispersion deposited on the water surface was determined based on the desired nanosheet density. For example, low-density nanosheet coatings were prepared with 50–100 μl of dispersion (containing 10 vol% ethanol) deposited on the surface of water in a polystyrene Petri dish (I.D. 35 mm) by using a Langmuir-Schaefer deposition method. High-density nanosheet coatings were obtained with 600 μl of dispersion (containing 5 vol% ethanol) deposited on the surface of water in a conical-shape TeflonTM trough (50-mm top I.D., 18-mm bottom I.D., and 26-mm

height) by using the floating-particle coating method.²⁸ The MFI nanosheet coatings on Si substrates were then calcined at 400 °C for 6 h with a ramp rate of 1 °C/min.

Removal of seeds from nanosheets after coating on Si substrates (seed-free nanosheet coatings). The nanocrystal seeds present at the center of the nanosheets were removed by mechanical rubbing to yield thin and oriented MFI nanosheet coatings. The calcined nanosheet coating on Si substrate was manually rubbed with a cotton fabric. For example, a nanosheet coating (1 cm × 1 cm) was rubbed with a finger wrapped with a cotton twill fabric 5–6 times in one direction. The rubbing process was repeated for another direction perpendicular to the first one. After rinsing with DI water, the coating on Si substrate was additionally calcined at 400 °C.

Secondary growth of MFI nanosheets MFI nanosheets coated on Si substrates were further grown by hydrothermal treatment in a TEAOH silica sol. The method was modified from the earlier reported one.³¹ Specifically, a sol with a composition of 1 TEOS: 0.1–0.3 TEAOH: 100 H₂O was hydrolyzed for 16 h under ambient conditions. Then, a Si substrate coated with MFI nanosheets was vertically placed in a TeflonTM-lined stainless steel autoclave that contained the TEAOH silica sol, by using a TeflonTM sample holder (Figure S1). After hydrothermal treatment at 130–170 °C, the sample was rinsed with ~10 ml of 0.1 M KOH solution and then thoroughly rinsed with copious amount of DI water.

For comparison, growth of MFI nanosheets was performed with a sol containing tetrapropylammonium hydroxide (TPAOH) and TEAOH, as previously reported.³¹ A sol with a composition of 1TEOS: 0.002TPAOH: 0.198TEAOH: 100H₂O was hydrolyzed for 16 h. Preheating of the sol was conducted with a TeflonTM-lined stainless steel autoclave at 150 °C for

2 h. After cooling, the sample was vertically placed in the autoclave and then heated at 90 °C for 2–3 days.

Fabrication of MFI films Large-grain, oriented, and thin MFI films were fabricated from seed-free MFI nanosheet coatings (i.e., after removing the seeds using mechanical rubbing, see above). It was determined that MFI nanosheet coatings after seed removal by rubbing did not grow with the TEAOH silica sol treatment and required TPAOH. Seed-free MFI nanosheet coatings were first grown with TPAOH/TEAOH silica sol at 90 °C for 3 days, after preheating at 150 °C for 2 h. The films were further treated with TEAOH silica sol (molar composition of 1 TEOS: 0.3 TEAOH: 100 H₂O) at 170 °C for 3 days twice to yield continuous MFI films with large grains. Thin MFI films were also prepared by 4 times TPAOH/TEAOH silica sol treatments of the seed-free MFI nanosheet coating at 90 °C for 3 days. The nanosheet coatings were calcined at 400 °C for 6 h with a ramp rate of 1 °C/min between each of the sol treatments for secondary growth. For comparison, MFI nanosheet coatings prepared without rubbing were grown with a TEAOH silica sol with a composition of 1 TEOS: 0.3 TEAOH: 100 H₂O at 170 °C for 4 days.

Characterization SEM images were acquired on JEOL 6700 or Hitachi SU8230. Measurements were typically performed with an operating voltage of 1.5 kV, while high-resolution images were recorded in a deceleration mode of SU8230 with 0.8 kV landing voltage. Focused ion beam milling was performed on FEI Quanta 200 3D to make a trench on the film for cross-sectional SEM measurements. TEM images were recorded on FEI Tecnai T12 with an accelerating voltage of 120 kV. For TEM imaging, MFI nanosheets were deposited on a copper grid with a carbon support film by using the Langmuir-Schaefer deposition method. AFM measurements were performed on Bruker Nanoscope V Multimode 8. AFM height images were recorded in tapping mode under ambient condition. Out-of-plane XRD patterns were recorded on

Panalytical X'Pert Pro diffractometer with Cu-K α radiation at 45 kV and 40 mA. Confocal fluorescence microscopy measurements were performed on Nikon A1Rsi confocal laser scanning fluorescence microscope with SIM Super Resolution. Trans-4-[4-(dimethylamino)styryl]-1-methylpyridinium iodide, fluorescent dye, was dissolved in ethanol (0.5 mM). Calcined MFI films on Si substrates were then mixed with the dye solution under vacuum, followed by heating at 70 °C for 1 day to infiltrate the dye into the micropores. The films were then gently rinsed with ethanol and dried under ambient condition. Confocal micrographs were acquired using a 561-nm illumination laser and a $60 \times /1.2$ NA water-immersion objective lens.

Results and Discussion

MFI nanosheets with high aspect ratios were prepared by a recently-reported direct synthesis method. 20 Figures 1a and b show a representative AFM height image and a TEM image of MFI nanosheets, respectively. The MFI nanosheet comprises a diamond-shape sheet and a seed nanocrystal located at the center of the sheet (a schematic is shown in Fig. 1c, where the seed crystal is shown in brown and the nanosheet in yellow). The size of the MFI nanosheets is typically \sim 1.2 and \sim 2 μ m in their in-plane short (along the c-axis) and long (along the a-axis) dimensions, respectively. The thickness of the nanosheet is mostly 5 nm (>60 % in area, Fig. 1a bottom), while the thickness at the center is often >100 nm. 20 The center thickening is attributed to the formation of MFI ad-layers and to the presence of the seed crystals. Figure S2 shows SEM images of large MFI nanosheets (\sim 3 μ m), which show obvious thickenings at the center. An earlier study established that these additional layers are formed by epitaxial growth, therefore sharing their crystallographic orientation with the nanosheet, 20 while the seed crystal is 90° rotated around the c-axis with respect to the nanosheet (i.e., it is a 90° rotational twin of the

nanosheet). An electron diffraction pattern of the MFI nanosheet (Fig. 1b, inset) reveals that the in-plane long and short dimensions are along the *a*- and *c*-axes, respectively, as schematically shown in Fig. 1c. This anisotropic shape of the MFI nanosheet allows to readily identify their in-plane crystallographic orientation.

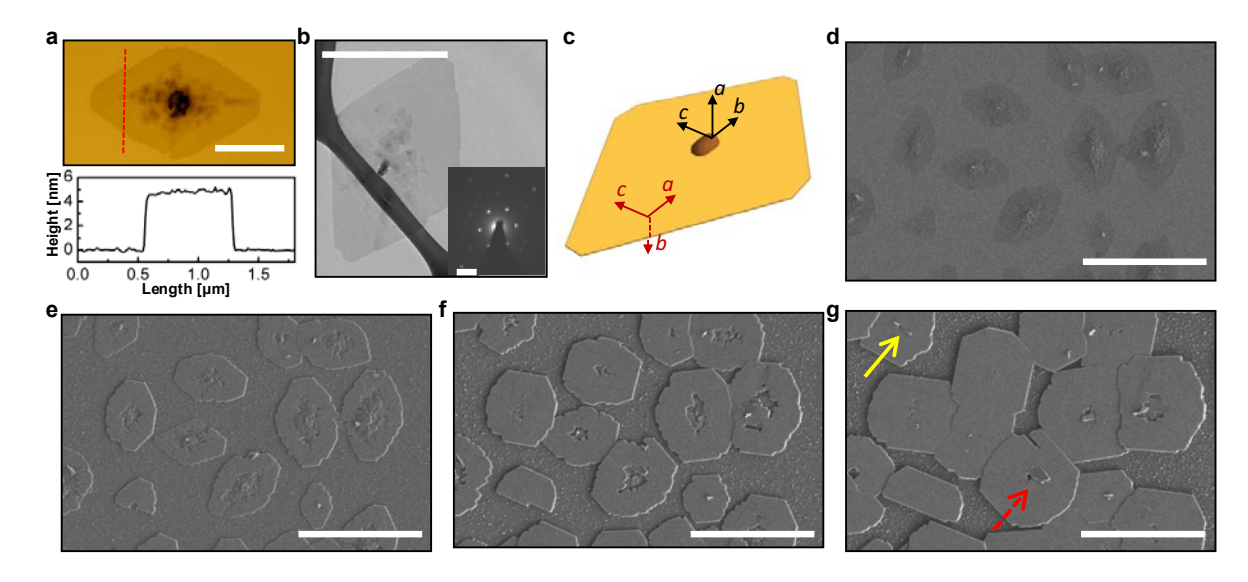


Figure 1. Representative a) AFM height image with a height profile along the indicated trace, b) TEM image with electron diffraction (ED) pattern (inset), c) schematic illustration, and d) a SEM image of MFI nanosheets on Si wafers. e–g) SEM images of MFI nanosheets on Si wafers collected from the location shown in (d) after 1–3 secondary growths in a TEAOH silica sol with a molar composition 1TEOS: 0.3 TEAOH: 100H₂O at 170 °C for 1 day. Scale bars are a) 1 μm, b) 1 μm (1 nm⁻¹ for the ED pattern shown in inset), and d–g) 5 μm. The red dotted line in a) indicates the positions from where the height profile was extracted. The crystallographic axes of MFI nanosheet and seed crystal at its center shown schematically in c) were determined earlier based on ED.²⁰ Protruding grains at the center of the nanosheets originating from a seed crystal and a central thick part are indicated by a solid yellow arrow and a dotted red arrow, respectively in (g).

Secondary growth of MFI nanosheets was investigated with the objective to fabricate oriented MFI thin films from nanosheet coatings. It was earlier demonstrated that TEAOH silica sols provide slow (a few nm/h) and highly anisotropic growth.³¹ Here, the TEAOH silica sol treatment was performed with higher TEAOH concentration at elevated temperature to increase the growth rate, so that the inter-nanosheet gaps can be filled within a reasonable time. A lowdensity MFI nanosheet coating on Si wafer was treated with TEAOH silica sol with a composition of 1TEOS: 0.3TEAOH: 100H₂O at 170 °C for 1 day. Figures 1d and e are SEM images of MFI nanosheets before and after TEAOH silica sol growth, respectively, acquired from the same location. The MFI nanosheets after a single treatment exhibit two distinguishable parts; the central and the peripheral part. The central part of the nanosheet contains the twin, aout-of-plane oriented seed crystal. This crystal evolves differently from the rest of the nanosheet during secondary growth and in part accounts for this contrast in morphology. Moreover, the central part of the nanosheet, because it is thicker than the periphery, causes the crystal to be slightly mis-oriented by not lying completely flat on the wafer, as the periphery does. This misorientation may also contribute to the morphology contrast.

The MFI nanosheet coating was repetitively treated with TEAOH silica sol, and the identical location was imaged to trace the morphology change of the nanosheets. Figure 1f shows a SEM image of MFI nanosheets treated twice with TEAOH silica sol at 170 °C for 1 day. Interestingly, the central parts have grown less than the rest of the nanosheet. After an additional treatment under the identical condition (Fig. 2g), the peripheral portion of the nanosheet expands and covers the central part, finally yielding a nearly flat crystal. Figure S3a shows a schematic of the nanosheet morphology evolution described above. The as-synthesized MFI nanosheet, which

initially has a complicated morphology, grows to yield flat crystals with well-developed facets, as the peripheral nanosheet portion overgrows on top of the central portion. This morphological evolution can be explained by considering that ad-layer formation on the (010)-face of MFI in TEAOH silica sols is 2D-nucleation limited, and therefore it is favored on flat surfaces.³¹ Due to the larger probability of nucleating a 2D nucleus, the flat periphery thickens faster than the central roughened region and eventually overgrows it. Although many of the crystals show completely flat surfaces, some still exhibit a rod-shape protrusion at their center (indicated by a solid yellow arrow in Fig. 1g). This is due to *a*-out-of-plane oriented seed twin growing fast along its *c*-direction (Fig. S3b). A protruding grain is also originated from the central thick part mis-oriented upon the coating on the substrate (indicated by a dotted red arrow in Fig. 1g, and schematically described in Fig. S3c). This morphology evolution, yielding finally flat grains, is considered desirable for thin film formation, as it results in a mostly *b*-oriented well-faceted single-crystal-like grain. For a conventional TPAOH silica sol treatment, the evolution of the nanosheet is very different, resulting in rough surfaces (Figure S4).

The in-plane long- and short-dimensions of the nanosheets correspond to the *a*- and *c*-axes, respectively, and, therefore, growth along these directions can be readily determined. Figure S5 shows results from nanosheets grown with a sol composition of 1 TEOS: 0.3 TEAOH: 100 H₂O at 170 °C for 4 days. Initially, a region of MFI nanosheet coating on Si substrate was imaged with SEM to record the initial lateral dimensions of MFI nanosheets (Fig. S5a). Then, the nanosheets were grown with TEAOH silica sol treatment, and the identical region of MFI nanosheet coating was imaged with SEM (Fig. S5b) and AFM (Fig. S5c) to establish the lateral dimensions and thicknesses, respectively.

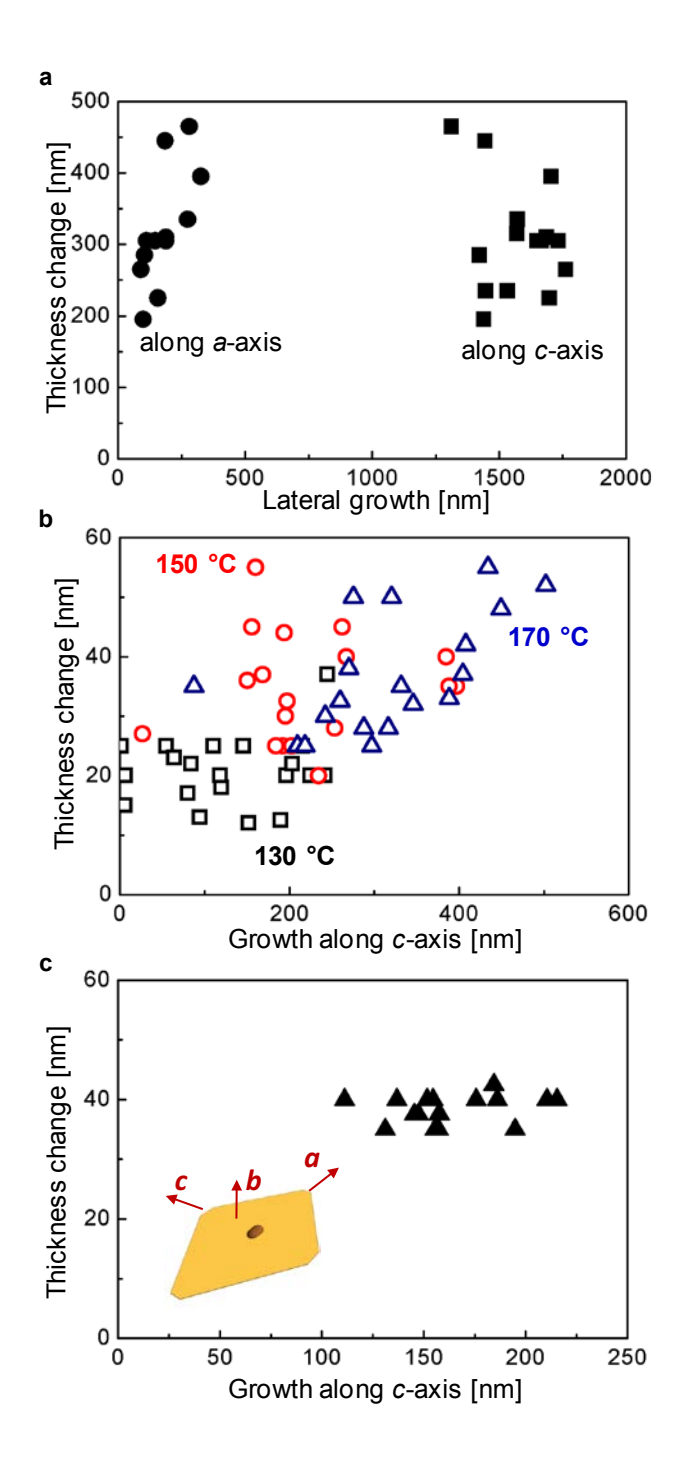


Figure 2. Growth measurement of MFI nanosheet along a, b, and c-axes under different treatment conditions. a) Thickness change (along b-axis) vs. lateral growth (\bullet : along a-axis, \bullet : along c-axis) of MFI nanosheets treated with a sol of molar composition 1TEOS: 0.3 TEAOH: 100 H₂O at 170 °C for 4 days. b) Thickness change (along b-axis) vs. growth along c-axis of

MFI nanosheets treated with a sol of molar composition 1TEOS: 0.1TEAOH: $100H_2O$ at 130 °C (\Box), 150 °C (\odot), and 170 ° (Δ) for 4 days. c) Thickness change (along *b*-axis) vs. growth along *c*-axis of MFI nanosheets treated with a sol of molar composition 1TEOS: 0.198TEAOH: 0.002TPAOH: $100H_2O$ at 90 °C for 2 days. Inset in Fig. 2c illustrates the crystallographic orientations of MFI nanosheet. Fig. 2b) and c) show only the lateral growth along *c*-axis, as the growth along *a*-axis is too small under these conditions to be precisely determined with SEM.

The change in size of MFI nanosheets after TEAOH silica sol treatment exhibits a wide distribution and therefore, it was measured for at least 10 nanosheets. Figure 2a shows thickness change (growth along b-axis) against the lateral growth (along a- and c-axis). Under this condition, the growth rate is sufficiently high to yield um-scale growth along c-axis (larger than the typical gap between MFI nanosheets in the monolayer coating). The widely scattered data, represented by the large standard deviations (43, 25, and 9% along a-, b- and c-axis, respectively), indicate inhomogeneities in crystal growth during TEAOH silica sol treatment. The average growths measured along a-, b-, and c- axes are 180, 320, and 1580 nm, respectively. This confirms that TEAOH sol treatment yields preferential growth along the c-axis of MFI, which is consistent with the previous report using exfoliated nanosheets.³¹ The current measurements provide more accurate comparison, due to straightforward assignment of crystallographic orientations. The growth rate along a-axis is comparable to or slightly lower than that along the b-axis. This is not desirable if we aim at creating an intergrown film with minimal thickening. However, the preferred growth along c-axis (lateral growth) is 5-fold larger than that along the b-axis and due to the random in-plane orientation of nanosheets, it can contribute in establishing an overall in-plane growth rate larger than the thickening rate. Also, we observe absence of twin formation, which is abundant under TPAOH secondary growth.

The preferred growth of MFI crystals along the c-axis was additionally confirmed for different TEAOH silica sol growth conditions. Growth measurements were conducted for MFI nanosheets grown with sol composition of 1 TEOS: 0.1 TEAOH: 100 H₂O at 130, 150, and 170 °C for 4 days (Figure S6), and their thickness changes vs. growth along the c-axis are shown in Figure 2b. Due to the reduced TEAOH concentrations and reaction temperatures, the nanosheets exhibit reduced growth, but they still show preferential growth along the c-axis. For example, TEAOH growth at 130 °C yielded average growth of 130 nm along the c-axis, while only 16 nm was observed for average thickness changes. In comparison, the growth along the a-axis was insignificant under these conditions (i.e., we could not measure the change precisely by SEM). In addition, the preferred growth along c-axis was also observed for secondary growth in TEAOH/TPAOH silica sols, as shown in Figure 2c. Interestingly, the thickness changes of MFI nanosheets exhibit a narrow distribution (standard deviation of 6%), indicating uniform thickening along the b-axis for different nanosheets. All growth assessment results are summarized in Table 1. The preferential growth along the c-axis compared to the growth along b-axis is consistently observed for all treatment conditions. This confirmed that the TEAOH silica sol growth is an attractive secondary growth method for the fabrication of b-oriented MFI thin films, as it yields preferred in-plane growth (along c-axis) on a b-oriented MFI nanosheet coating without twining.

Table 1. Average ratios of growth along *c*-axis to *b*-axis for MFI nanosheets treated with TEAOH or TPAOH/TEAOH silica sol under various conditions

Sol composition	Reaction temperature	Reaction time	Ratio of growth along c- to b-axis
1TEOS: 0.3 TEAOH : 100 H ₂ O	170 °C	4 days	5.4 ±1.3
1TEOS: 0.1 TEAOH : $100~\text{H}_2\text{O}$	130 °C	4 days	9.1 ±6.8
1TEOS: 0.1 TEAOH : 100 H ₂ O	150 °C	4 days	8.1 ±3.9
1TEOS: 0.1 TEAOH : $100~\text{H}_2\text{O}$	170 °C	4 days	10.4 ±2.9
1TEOS: 0.198 TEAOH : 0.002 TPAOH : 100 H $_2$ O	90 °C	2 days	4.3 ±0.7

The use of TEAOH sol growth method was explored for its ability to enable oriented MFI thin film fabrication from the directly-synthesized nanosheets. Although a fully intergrown film with a thickness of \sim 200 nm can be prepared from a dense nanosheet monolayer coating (Figure S7), the film also contains rod-shaped crystals shooting out from the center of the nanosheets. They originate from the seed nanocrystals present at the central part of the nanosheets, which due to the larger central thickness are sitting inclined on the support and, under TEAOH secondary growth, grow fast along their c-axis.

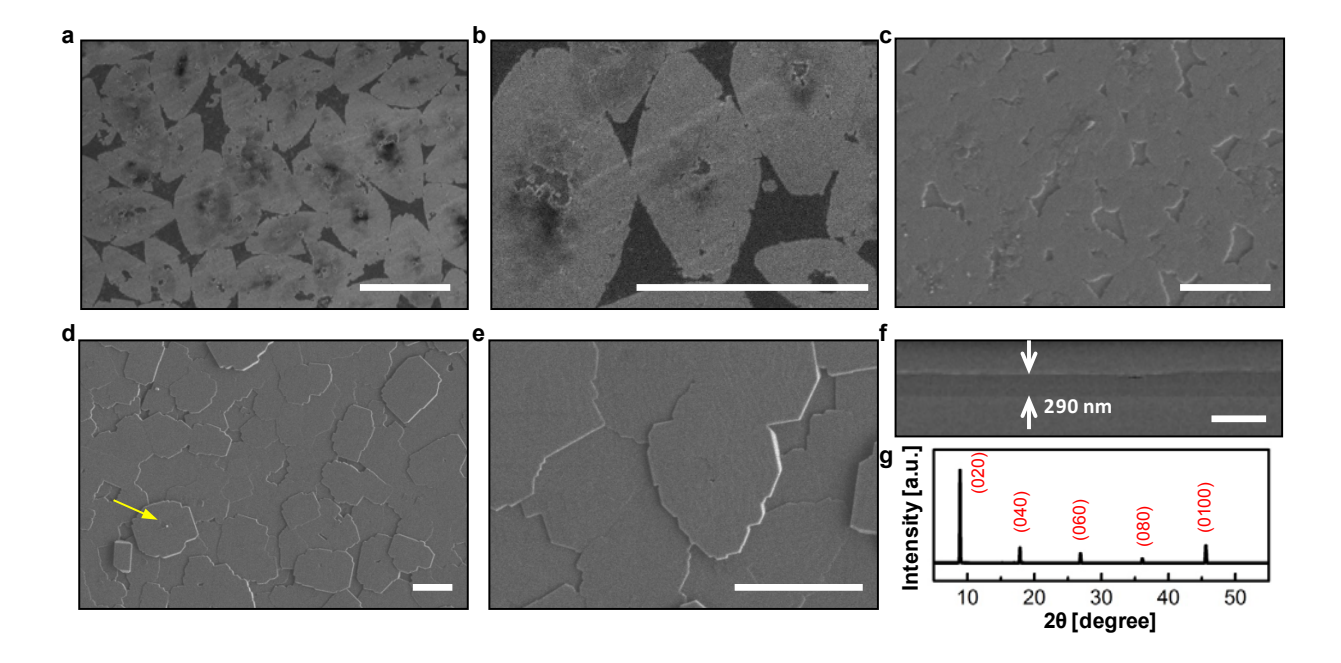


Figure 3. SEM images of seed-free MFI nanosheet coating (prepared by rubbing) a,b) before and c) after secondary growth with a sol of molar composition 1TEOS: 0.198TEAOH: 0.002TPAOH: 100H₂O at 90 °C for 3 days; and d,e,f) two additional TEAOH sol treatments (1 TEOS: 0.3 TEAOH: 100 H₂O at 170 °C for 3 days, each) to yield continuous MFI films with large and flat grains (d.e: top view, f: cross-sectional view). This film has few mis-oriented grains (one is indicated by a yellow arrow in d). g) XRD pattern of MFI film shown in d–f. Scale bars are a–e) 2 μm and f) 500 nm.

In order to reduce mis-oriented grains, MFI nanosheets were synthesized with reduced ethanol content (hydrolysis under air purging) and reduced reaction time (e.g., 32 h) to minimize the central thickening, allowing for the seed nanocrystals to be removed from the coating by mechanical rubbing with cotton fabric.²⁰ Figure 3a shows a SEM image of a MFI nanosheet coating on Si substrate after rubbing. Seed nanocrystals at the center of the nanosheets were detached, leaving holes behind. This rubbing process can effectively remove the seeds at the center of the nanosheets and also excess seed crystals (not connected to the nanosheets) from the nanosheet coatings. Scratches, probably due to the seed nanocrystals detached from the nanosheets, were evident, indicating mechanical damage on the MFI nanosheets during the rubbing (Figure 3b). This damage appears to be detrimental to the secondary growth, as no growth was observed for the rubbed nanosheets treated with TEAOH silica sol (Figure S8). It was suggested earlier that TEAOH silica sol growth of MFI crystals relies on 2D nucleation of ad-layers followed by their in-plane propagation, and it was observed that even small deviations from the nominal structure (e.g., the curvature of nanosheets caused by their overlap) can effectively suppress the step propagation.³¹ Apparently, the surface damage induced by the rubbing is a sufficient hurdle that hinders the crystal growth under TEAOH sol treatment.

Using a TPAOH/TEAOH silica sol, it was possible to grow the rubbed (seed-free) MFI nanosheets. Figure 3c shows a SEM image of MFI nanosheets treated with TPAOH/TEAOH silica sol at 90 °C for 3 days, after preheating of the precursor sol. Growth of MFI nanosheets is evident without any hint of scratches, while the holes at the center were not fully filled.

After the first TPAOH/TEAOH sol treatment of seed-free MFI nanosheets, additional TEAOH silica sol treatments were utilized. Figure S9 shows SEM images of an MFI film fabricated by a TPAOH/TEAOH treatment followed by a TEAOH silica sol treatment at 170 °C 3 days. It shows

obvious growth of grains and establishes that any surface damage has been repaired by the single TPAOH/TEAOH silica sol growth. As the film still possesses unfilled gaps (i.e., gaps between nanosheets facing each other along their a-axes) and remaining holes at the center of grains, a second TEAOH silica sol growth was performed for the film under identical conditions. Figures 3d and e are SEM images of the MFI film obtained after the second TEAOH silica sol treatment. It confirms that the grains are fully intergrown. Although a few mis-oriented grains are still observed (indicated by a yellow arrow), most grains are large (>2 µm) and flat. The rubbing process effectively removed seed crystals, and rod-like crystals are not observed from this film. Fig. 3f is a cross-sectional SEM image of the film and confirms the thickness of the film is ~300 nm. This is inevitable thickening of the film, as the gap size between the nanosheets increases with the size of nanosheet. Therefore, the seed coating with large-size nanosheets requires large extent of secondary growth to fill the gaps, compared to the nanosheet coating from exfoliated nanosheets with a few hundred nanometer lateral dimensions.³⁵ The XRD pattern of this MFI film shows intense (0k0) reflections, establishing that the film is highly oriented (Fig. 3g). For comparison, an MFI film was fabricated from a seed-free nanosheet coating with four times treatments with TPAOH/TEAOH silica sol (Fig. S10). Although this method yielded a thin (~170 nm) and b-out-of-plane oriented MFI film, SEM shows the presence of some mis-oriented grains and confirms that the TPAOH/TEAOH silica sol treatment cannot yield single-crystal-like grains.

An MFI film fabricated from the seed-free nanosheet coating was compared with a film fabricated from the seed-containing nanosheet coating by confocal fluorescence microscopy. The identical position of an MFI film fabricated from seed-containing nanosheet coating treated with TEAOH silica sol was imaged by SEM (Fig. 4a) and confocal fluorescence microscopy (Fig.

4b). The contrast of the signal intensities between the grains allows to identify each grain in the confocal micrograph. Elongated crystals, originated from the seed nanocrystals, appear bright and are clearly identifiable at the center of the grains. Some of the grains, with flat single-crystal like appearance in the SEM, reveal by confocal microscopy diamond-shaped dark regions at the center, which can be attributed to the mis-oriented central parts of the nanosheets. In contrast, the MFI film prepared from the seed-free nanosheet coating shows much simpler microstructures. The confocal image of the film (Fig. 4d) shows similar morphology with that observed in SEM image (Fig. 4c), establishing that mostly ~2-μm continuous grains comprise the film with very few detectable mis-oriented grains. This uniform microstructure could serve as a starting point for improved-performance molecular-sieve separation membranes.

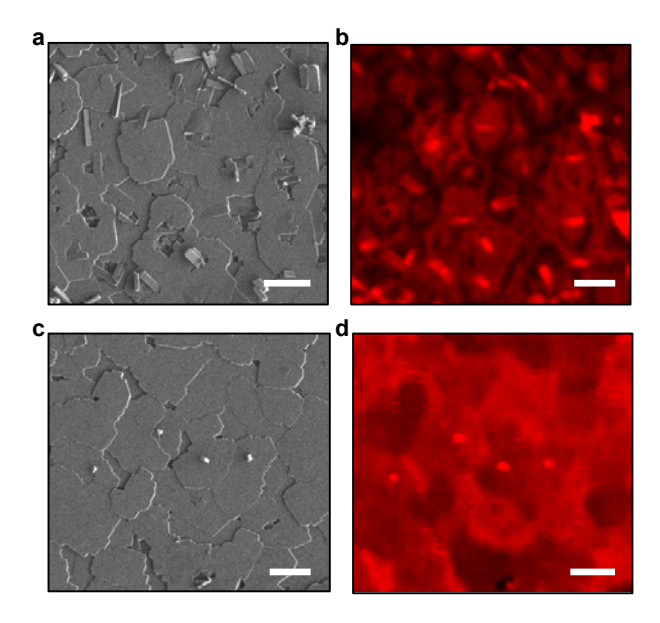


Figure 4. a,c) SEM images and b,d) confocal fluorescence microscopy images of MFI films fabricated from a,b) seed-containing and c,d) seed-free (rubbed) MFI nanosheet coatings. Scale bars indicate 2 μm.

Conclusion

The secondary growth of directly-synthesized MFI nanosheets in TEAOH silica sols was investigated to fabricate b-oriented MFI thin films with large grains. Twining-free preferential growth of MFI nanosheets along c-axis (a lateral direction of the nanosheet) during TEAOH silica sol treatment was confirmed and utilized to intergrow MFI nanosheet monolayers on Si wafers into continuous and oriented films. In addition, nanocrystal seeds at the center of MFI nanosheets were removed by rubbing to eliminate the mis-oriented portion of the nanosheet coatings. When sequentially subjected to a TPAOH/TEAOH silica sol treatment followed by a TEAOH silica sol treatments, these seed-removed monolayer coatings yield large-grain (\sim 2 μ m), b-out-of-plane oriented, and thin (\sim 300 nm) MFI films on Si wafers.

ASSOCIATED CONTENT

Supporting Information. The supporting information is available free of charge via the Internet

at http://pubs.acs.org.

SEM images of MFI nanosheets before and after silica sol treatments with TPAOH and/or

TEAOH, schematics for TEAOH silica sol growth of MFI nanosheets, and growth assessment

results performed with TEAOH sol, characterization of MFI thin films (PDF)

AUTHOR INFORMATION

Corresponding Author

*E-mail: tsapa001@umn.edu

ORCID

Donghun Kim: 0000-0003-4080-5869

Meera Shete: 0000-0002-4269-2688

Michael Tsapatsis: 0000-0001-5610-3525

Notes

The authors declare no competing financial interest.

ACKNOWLEDGMENT

This work was partially supported by the Center for Gas Separations Relevant to Clean Energy

Technologies, an Energy Frontier Research Center funded by the US Department of Energy,

Office of Science, Basic Energy Sciences under Award DE-SC0001015 for the preparation of

MFI nanosheets and films and by the National Science Foundation (CBET-1705687) for the film

microstructure characterization. Characterization was carried out in the Characterization Facility,

18

University of Minnesota and the Minnesota Nano Center, which receive partial support from the NSF through the MRSEC and NNIN programs, respectively. Part of SEM measurements was performed on a Hitachi 8230 provided by NSF MRI DMR-1229263. Confocal microscopy measurement was conducted at the University of Minnesota - University Imaging Center.

REFERENCES

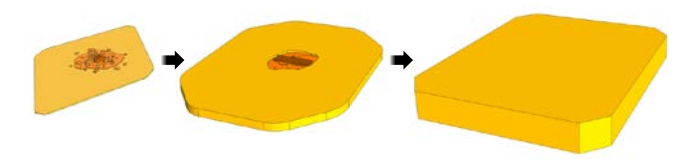
- (1) Davis, M. E. Ordered Porous Materials for Emerging Applications. *Nature* **2002**, *417*, 813–821.
- (2) Corma, A. State of the Art and Future Challenges of Zeolites as Catalysts. *J. Catal.* **2003**, *216*, 298–312.
- (3) Lew, C. M.; Cai, R.; Yan, Y. Zeolite Thin Films: From Computer Chips to Space Stations. *Acc. Chem. Res.* **2010**, *43*, 210–219.
- (4) Pina, M. P.; Mallada, R.; Arruebo, M.; Urbiztondo, M.; Navascués, N.; Iglesia, O. de la; Santamaria, J. Zeolite Films and Membranes. Emerging Applications. *Microporous Mesoporous Mater.* 2011, 144, 19–27.
- (5) Gascon, J.; Kapteijn, F.; Zornoza, B.; Sebastián, V.; Casado, C.; Coronas, J. Practical Approach to Zeolitic Membranes and Coatings: State of the Art, Opportunities, Barriers, and Future Perspectives. *Chem. Mater.* 2012, 24, 2829–2844.
- (6) Caro, J.; Noack, M. Zeolite Membranes Recent Developments and Progress. *Microporous Mesoporous Mater.* 2008, 115, 215–233.
- (7) Rangnekar, N.; Mittal, N.; Elyassi, B.; Caro, J.; Tsapatsis, M. Zeolite Membranes a Review and Comparison with MOFs. *Chem. Soc. Rev.* **2015**, *44*, 7128–7154.
- (8) Wang, Z.; Wang, H.; Mitra, A.; Huang, L.; Yan, Y. Pure-Silica Zeolite Low-k Dielectric Thin Films. *Adv. Mater.* **2001**, *13*, 746–749.
- (9) Volksen, W.; Miller, R. D.; Dubois, G. Low Dielectric Constant Materials. *Chem. Rev.* **2010**, *110*, 56–110.
- (10) Choi, J.; Lai, Z.; Ghosh, S.; Beving, D. E.; Yan, Y.; Tsapatsis, M. Layer-by-Layer Deposition of Barrier and Permselective *c*-Oriented-MCM-22/ Silica Composite Films. *Ind. Eng. Chem. Res.* 2007, 46, 7096–7106.
- (11) Cai, R.; Sun, M.; Chen, Z.; Munoz, R.; O'Neill, C.; Beving, D. E.; Yan, Y. Ionothermal Synthesis

- of Oriented Zeolite AEL Films and Their Application as Corrosion-Resistant Coatings. *Angew. Chem. Int. Ed.* **2008**, *47*, 525–528.
- (12) Cai, R.; Yan, Y. Corrosion-Resistant Zeolite Coatings. Corrosion 2008, 64, 271–278.
- (13) O'Neill, C.; Beving, D. E.; Chen, W.; Yan, Y. Durability of Hydrophilic and Antimicrobial Zeolite Coatings under Water Immersion. *AIChE J.* **2006**, *52*, 1157–1161.
- (14) Xu, X.; Wang, J.; Long, Y. Zeolite-Based Materials for Gas Sensors. Sensors 2006, 6, 1751–1764.
- (15) Sahner, K.; Hagen, G.; Schönauer, D.; Reiß, S.; Moos, R. Zeolites Versatile Materials for Gas Sensors. *Solid State Ionics* **2008**, *179*, 2416–2423.
- (16) Boscoboinik, J. A.; Yu, X.; Yang, B.; Fischer, F. D.; Włodarczyk, R.; Sierka, M.; Shaikhutdinov, S.; Sauer, J.; Freund, H.-J. Modeling Zeolites with Metal-Supported Two-Dimensional Aluminosilicate Films. *Angew. Chem. Int. Ed.* 2012, 51, 6005–6008.
- (17) Kestell, J. D.; Zhong, J.; Shete, M.; Waluyo, I.; Sadowski, J. T.; Stacchiola, D. J.; Tsapatsis, M.; Boscoboinik, J. A. Studying Two-Dimensional Zeolites with the Tools of Surface Science: MFI Nanosheets on Au(111). Catal. Today 2017, 280, 283–288.
- (18) Hedlund, J.; Sterte, J.; Anthonis, M.; Bons, A. J.; Carstensen, B.; Corcoran, N.; Cox, D.; Deckman, H.; De Gijnst, W.; de Moor, P. P.; et al. High-Flux MFI Membranes. *Microporous Mesoporous Mater.* **2002**, *52*, 179–189.
- (19) Lai, Z.; Bonilla, G.; Diaz, I.; Nery, J. G.; Sujaoti, K.; Amat, M. A.; Kokkoli, E.; Terasaki, O.; Thompson, R. W.; Tsapatsis, M.; et al. Microstructural Optimization of a Zeolite Membrane for Organic Vapor Separation. *Science* 2003, 300, 456–460.
- (20) Jeon, M. Y.; Kim, D.; Kumar, P.; Lee, P. S.; Rangnekar, N.; Bai, P.; Shete, M.; Elyassi, B.; Lee, H. S.; Narasimharao, K.; et al. Ultra-Selective High-Flux Membranes from Directly Synthesized Zeolite Nanosheets. *Nature* 2017, 543, 690–694.
- (21) Fu, D.; Schmidt, J. E.; Ristanović, Z.; Chowdhury, A. D.; Meirer, F.; Weckhuysen, B. M. Highly

- Oriented Growth of Catalytically Active Zeolite ZSM-5 Films with a Broad Range of Si/Al Ratios. Angew. Chem. Int. Ed. **2017**, *56*, 11217–11221.
- (22) Snyder, M. A.; Tsapatsis, M. Hierarchical Nanomanufacturing: From Shaped Zeolite Nanoparticles to High-Performance Separation Membranes. *Angew. Chem. Int. Ed.* 2007, 46, 7560–7573.
- (23) Tsapatsis, M.; Okubo, T.; Lovallo, M.; Davis, M. E. Synthesis and Structure of Ultrafine Zeolite KL (LTL) Crystallites and Their Use for Thin Film Zeolite Processing. *MRS Proc.* **1994**, *371*, 21.
- (24) Gouzinis, A.; Tsapatsis, M. On the Preferred Orientation and Microstructural Manipulation of Molecular Sieve Films Prepared by Secondary Growth. *Chem. Mater.* **1998**, *10*, 2497–2504.
- (25) Yuan, W.; Lin, Y. S.; Yang, W. Molecular Sieving MFI-Type Zeolite Membranes for Pervaporation Separation of Xylene Isomers. *J. Am. Chem. Soc.* **2004**, *126*, 4776–4777.
- (26) Drews, T. O.; Tsapatsis, M. Progress in Manipulating Zeolite Morphology and Related Applications. *Curr. Opin. Colloid Interface Sci.* **2005**, *10*, 233–238.
- (27) Yoon, K. B. Organization of Zeolite Microcrystals for Production of Functional Materials. *Acc. Chem. Res.* **2007**, *40*, 29–40.
- (28) Kim, D.; Jeon, M. Y.; Stottrup, B. L.; Tsapatsis, M. Para-Xylene Ultra-Selective Zeolite MFI Membranes Fabricated from Nanosheet Monolayers at the Air-Water Interface. *Angew. Chem. Int.* Ed. 2018, 57, 480–485.
- (29) Pham, T. C. T.; Kim, H. S.; Yoon, K. B. Growth of Uniformly Oriented Silica MFI and BEA Zeolite Films on Substrates. *Science* **2011**, *334*, 1533–1538.
- (30) Pham, T. C. T.; Nguyen, T. H.; Yoon, K. B. Gel-Free Secondary Growth of Uniformly Oriented Silica MFI Zeolite Films and Application for Xylene Separation. *Angew. Chem. Int. Ed.* 2013, 52, 8693–8698.
- (31) Shete, M.; Kumar, M.; Kim, D.; Rangnekar, N.; Xu, D.; Topuz, B.; Agrawal, K. V.; Karapetrova,

- E.; Stottrup, B.; Al-Thabaiti, S.; et al. Nanoscale Control of Homoepitaxial Growth on a Two-Dimensional Zeolite. *Angew. Chem. Int. Ed.* **2017**, *56*, 535–539.
- (32) Peng, Y.; Lu, X.; Wang, Z.; Yan, Y. Fabrication of *b*-Oriented MFI Zeolite Films under Neutral Conditions without the Use of Hydrogen Fluoride. *Angew. Chem. Int. Ed.* **2015**, *54*, 5709–5712.
- (33) Varoon, K.; Zhang, X.; Elyassi, B.; Brewer, D. D.; Gettel, M.; Kumar, S.; Lee, J. A.; Maheshwari, S.; Mittal, A.; Sung, C. Y.; et al. Dispersible Exfoliated Zeolite Nanosheets and Their Application as a Selective Membrane. *Science* 2011, 334, 72–75.
- (34) Choi, M.; Na, K.; Kim, J.; Sakamoto, Y.; Terasaki, O.; Ryoo, R. Stable Single-Unit-Cell Nanosheets of Zeolite MFI as Active and Long-Lived Catalysts. *Nature* **2009**, *461*, 246–249.
- (35) Rangnekar, N.; Shete, M.; Agrawal, K. V.; Topuz, B.; Kumar, P.; Guo, Q.; Ismail, I.; Alyoubi, A.; Basahel, S.; Narasimharao, K.; et al. 2D Zeolite Coatings: Langmuir-Schaefer Deposition of 3 nm Thick MFI Zeolite Nanosheets. *Angew. Chem. Int. Ed.* 2015, 54, 6571–6575.
- (36) Tiriolo, R.; Rangnekar, N.; Zhang, H.; Shete, M.; Bai, P.; Nelson, J.; Karapetrova, E.; Macosko, C. W.; Siepmann, J. I.; Lamanna, E.; et al. Sub-Micrometer Zeolite Films on Gold-Coated Silicon Wafers with Single-Crystal-Like Dielectric Constant and Elastic Modulus. *Adv. Funct. Mater.* 2017, 27, 1700864.

Table of Contents



Large-grain, oriented, and thin zeolite MFI films from directly-synthesized nanosheet coatings

Donghun Kim, Meera Shete, Michael Tsapatsis*

Department of Chemical Engineering and Materials Science, University of Minnesota, Minneapolis, Minnesota 55455 United States

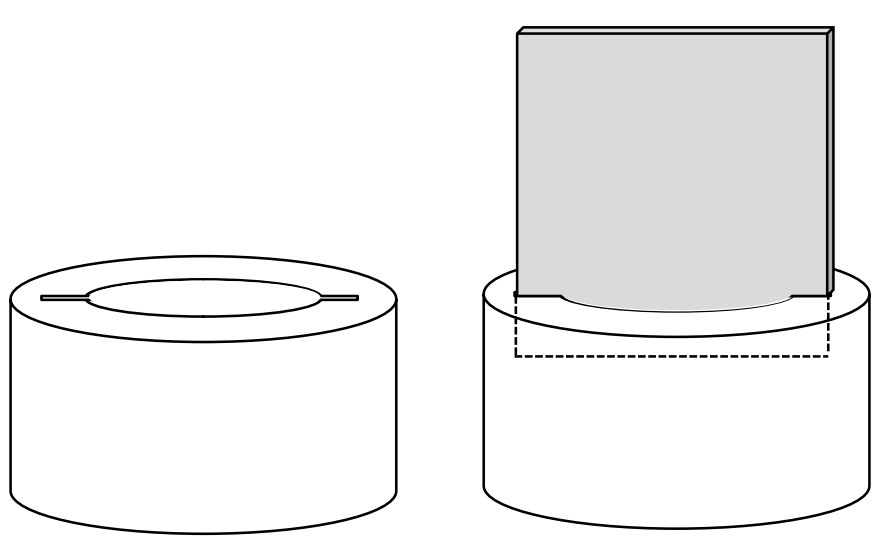


Figure S1. Schematic illustration of a TeflonTM sample holder to vertically place a Si substrate in a TeflonTM-lined stainless-steel autoclave.

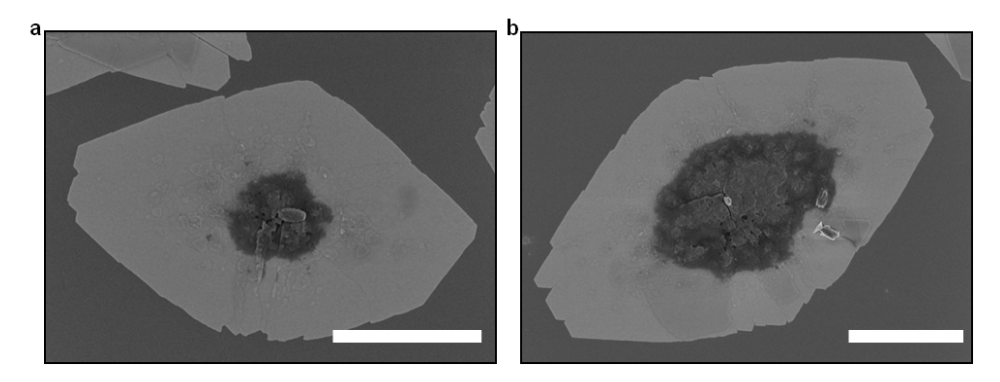


Figure S2. High resolution SEM images of MFI nanosheets. Ad-layers are predominantly formed near the central part of the nanosheets, resulting in thick centers (>100 nm) for nanosheets that are larger than 3 μ m in lateral dimension. Scale bars are 1 μ m.

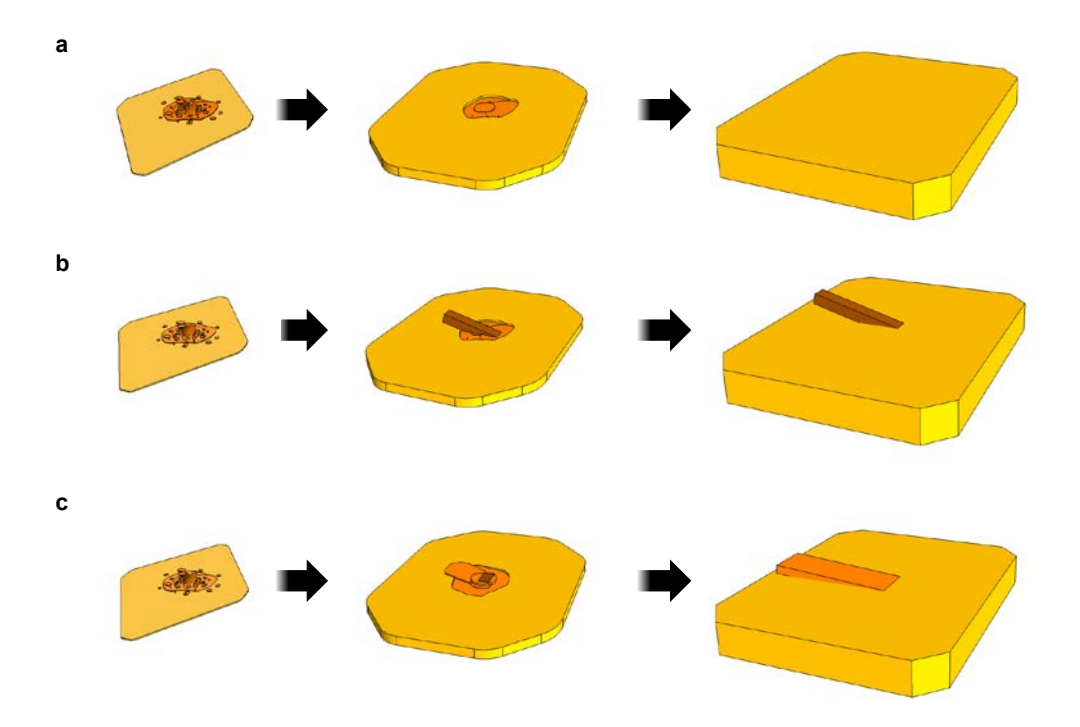


Figure S3 Schematic illustrations of observed MFI nanosheet evolution during TEAOH silica sol treatment.

- a) The peripheral nanosheet grows faster than the central thick portion, and the nanosheet eventually becomes a flat grain.
- b) In comparison, some nanosheets grow with protruding grains at the center. A mis-oriented seed crystal at the center of the nanosheet grows along the c-axis before it is covered by the fast-growing nanosheet, yielding a rod-shape protruding grain.
- c) Some mis-oriented central thick parts of the nanosheets may also yield protruding grains.

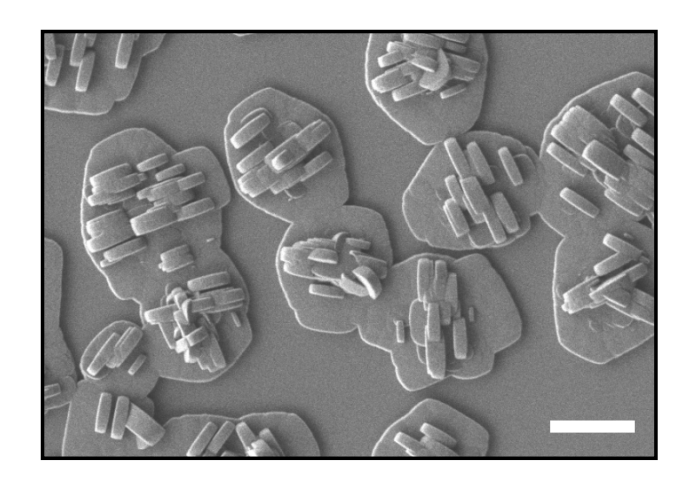


Figure S4 SEM image of MFI nanosheets grown with TPAOH silica sol treatment with a molar composition of 60 SiO₂: 9TPAOH: 9500 H_2O : 240 EtOH at 90 °C for 4 days.¹ Scale bar represents 2 μm .

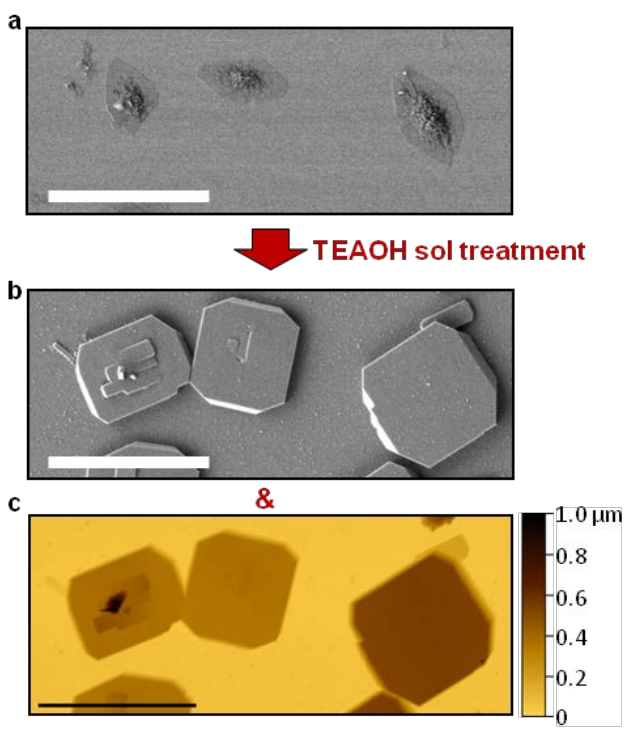


Figure S5. Growth measurement for MFI nanosheets treated with TEAOH silica sol of molar composition 1TEOS: 0.3TEAOH: $100H_2O$. a) SEM image of initial MFI nanosheets, and b) SEM image and c) AFM height image of MFI nanosheets after TEAOH silica sol growth at $170~^{\circ}C$ for 4 days. SEM images and AFM height image were collected at the identical position of the sample. Scale bars represent 5 μ m.

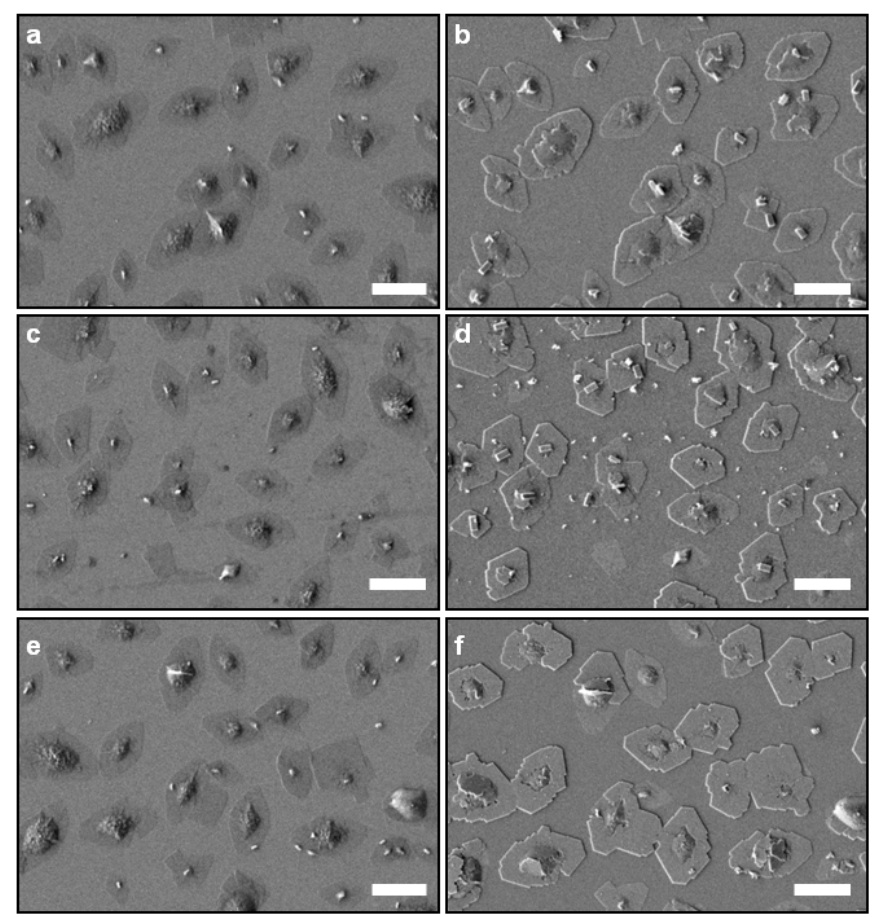


Figure S6. SEM images before (a,c,e) and after (b,d,f) TEAOH sol growth of MFI nanosheets at different temperatures for 4 days: b) 130 °C, d) 150 °C, and f) 170 °C. The molar composition of TEAOH silica sol is 1TEOS: 0.1 TEAOH: 100H₂O. The corresponding SEM images were acquired from identical positions. Scale bars indicate 2 μm.

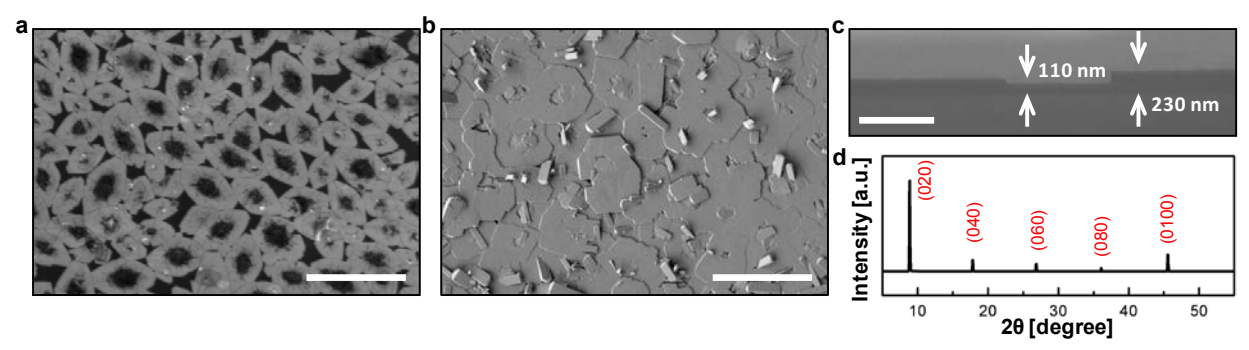


Figure S7. a) SEM image of MFI nanosheet monolayer coating and b) top-view and c) cross-sectional SEM images of MFI film fabricated by TEAOH silica sol treatment (1 TEOS: 0.3 TEAOH: $100~H_2O$ at $170~^{\circ}C$ for 3 days). d) XRD pattern of the MFI film shown in panel b and c. Scale bars are a,b) 5 μ m and c) 500 nm.

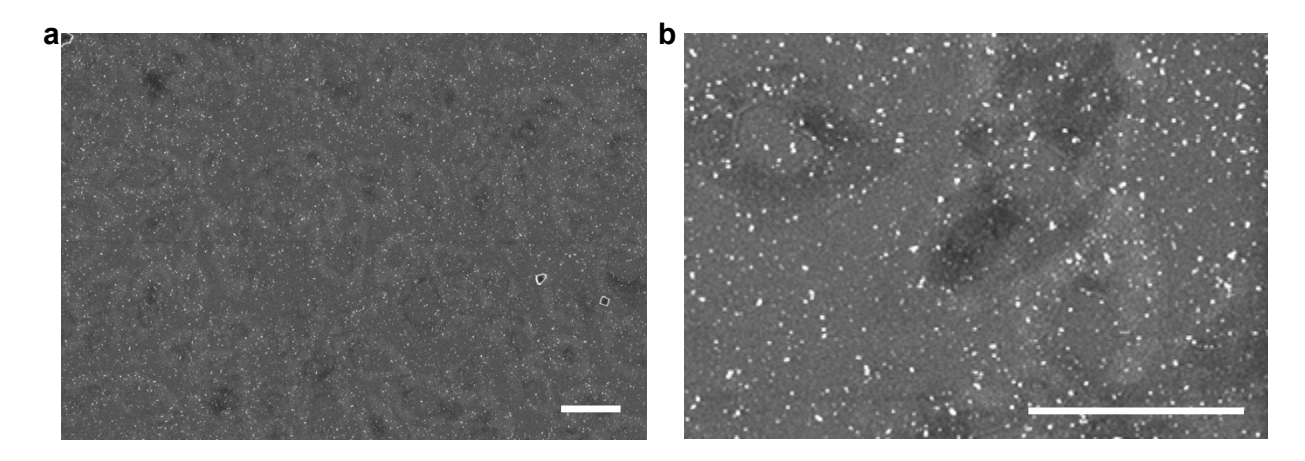


Figure S8. SEM images of seed-free (rubbed) MFI nanosheet coating treated with a sol of composition 1 TEOS: 0.3 TEAOH: 100 $_{2}$ O at 170 $_{2}$ O at 170 $_{2}$ O for 4 days. The nanosheets after the seed-removal by rubbing do not grow under TEAOH silica sol treatment. Scale bars indicate 2 $_{1}$ m.

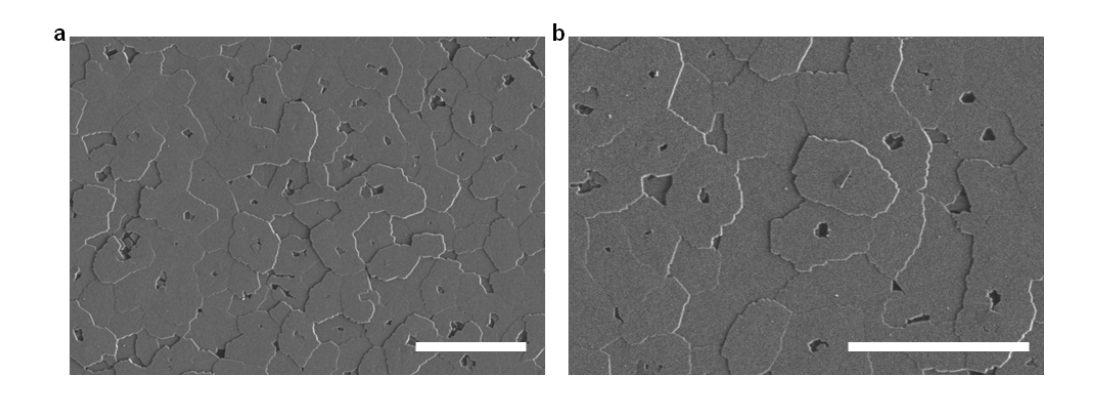


Figure S9. SEM images of an MFI film fabricated from a seed-free nanosheet coating, sequentially grown with a TPAOH/TEAOH sol treatment and a TEAOH sol treatment. Scale bars are $5~\mu m$.

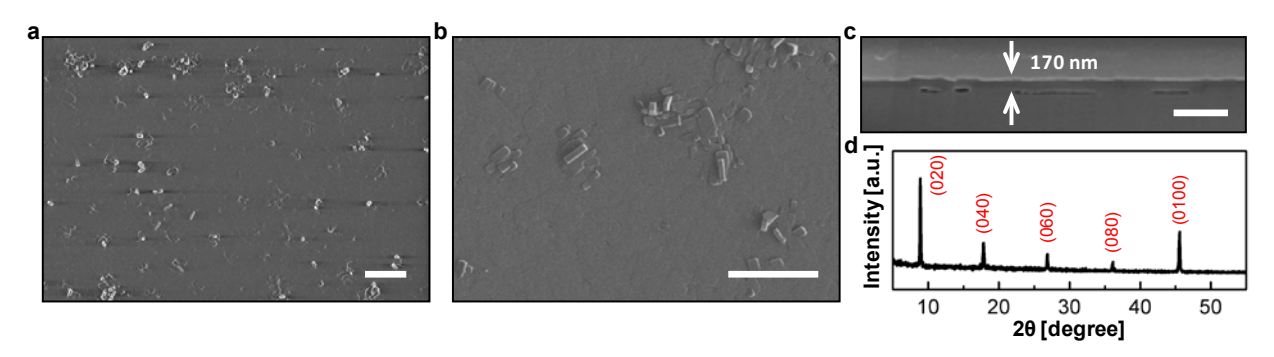


Figure S10. a,b) Top-view and c) cross-sectional view SEM images, and d) XRD pattern of MFI film fabricated from seed-free MFI nanosheet coating with 4-times treatments with a sol of molar composition 1TEOS: 0.198 TEAOH: 0.002TPAOH: 100H₂O at 90 °C. The scale bars are a,b) 2 μm and c) 500 nm.

REFERENCE

(1) Choi, J.; Ghosh, S.; Lai, Z.; Tsapatsis, M. Uniformly a-Oriented MFI Zeolite Films by Secondary Growth. *Angew. Chem. Int. Ed.* **2006**, *45*, 1154–1158.